

Contingency Detection in Modern Power Systems: A Stochastic Hybrid System Method

Shuo Yuan, Le Yi Wang, *Life Fellow, IEEE*, George Yin, *Life Fellow, IEEE*, Masoud H. Nazari, *Senior Member, IEEE*

Abstract—This paper introduces a new stochastic hybrid system (SHS) framework for contingency detection in modern power systems (MPS). The framework uses stochastic hybrid system representations in state space models to expand and facilitate capability of contingency detection. In typical microgrids (MGs), buses may contain various synchronous generators, renewable generators, controllable loads, battery systems, regular loads, etc. For development of SHS models in power systems, this paper introduces the concept of dynamic and non-dynamic buses. By converting a physical power grid into a virtual linearized state space model and representing contingencies as random switching of system structures and parameters, this paper formulates the contingency detection problem as a joint estimation problem of discrete event and continuous states in stochastic hybrid systems. This method offers unique advantages, including using common measurement signals on voltage and current synchrophasors to detect different types and locations of contingencies, avoiding expensive local direct fault measurements and detecting certain contingencies that cannot be directly measured. The method employs a small and suitably-designed probing signal to sustain the ability of persistent contingency detection. Joint estimation algorithms are presented with their proven convergence and reliability properties. Examples that use an IEEE 5-bus system demonstrate the main ideas and derivation steps. Simulation case studies on an IEEE 33-bus system are used for detecting transmission line faults and sensor interruptions.

Index Terms—Modern power system, contingency detection, stochastic hybrid system, state estimation, reliability, convergence.

I. INTRODUCTION

Reliability of modern power systems (MPS) mandates fast and accurate detection of cyber-physical contingencies in diversified categories, including line faults, generator failures, sensor malfunctions, communication system disruptions, among many others [1]. Contingency detection in power systems is a critical and challenging task. Power system contingencies include physical faults such as transmission line faults, information failures such as communication channel interruptions and sensor faults, and intentional cyber attacks that alter system structures and parameters.

Shuo Yuan is with the Department of Electrical and Computer Engineering, Wayne State University, Detroit, Michigan 48202, USA <shuoyuan@wayne.edu>

Le Yi Wang is with the Department of Electrical and Computer Engineering, Wayne State University, Detroit, Michigan 48202, USA <lywang@wayne.edu>

George Yin is with the Department of Mathematics, University of Connecticut, Storrs, Connecticut 06269-1009, USA <gyin@uconn.edu>

Masoud Nazari is with the Department of Electrical and Computer Engineering, Wayne State University, Detroit, Michigan 48202, USA <masoud.nazari@wayne.edu>

Traditionally, unique and dedicated local sensors and switching circuits have been designed and implemented at numerous locations on transmission lines, buses, generators, and users. These detection devices are exemplified by power line sensors, faulty circuit indicators, fault passage indicators, over-current relays, and so on. Enhancement of reliability can also be achieved by using existing sensor systems with advanced detection methodologies and algorithms [2]–[4].

This paper introduces a new approach that employs system dynamics and their switching for enhancing and expanding the capability of contingency detection. This approach offers several appealing advantages. For example, an existing sensor such a phasor measurement unit (PMU) or a current sensor on a bus can be used to detect many types and different locations of contingencies. This much enhanced capability is achieved by embedding contingencies within dynamic systems so that a switching from a normal operating condition to a faulty condition caused by a contingency can be detected as two different dynamic systems. This leads to the stochastic hybrid system (SHS) framework of power systems. This new framework for modeling power systems was introduced in the companion paper [5] that treats also state estimation problems. This paper is focused on contingency detection. Since this approach must rely on system dynamics to detect contingency and estimate state simultaneously, they face numerous challenges. This paper aims to resolve these challenges and introduce useful algorithms in the SHS framework.

This paper considers power grids whose buses may contain various traditional synchronous generators and renewable generators, controllable loads, energy storage systems, battery systems, regular loads, and so on. Their system dynamics are represented by nonlinear state space models. Contingencies are represented by jumps in system structures (such as loss of a transmission line, loss of communication channel in an interval), model parameters (such as impedance jumps in transmission lines and generation parameters), loss of a member (loss of a load cluster on a bus), among many other scenarios. Most power system contingencies occur randomly. Adding such random jumps into dynamic models of MGs, the system models become stochastic state-space hybrid systems.

Due to their critical importance, contingency detection and state estimation problems in power systems have been investigated extensively. For example, the reference [6] proposed a support vector machine-based fault localization methodology to identify and localize transmission line faults occurring at any location in a power grid based on PMUs (phasor measurement units) measurements. A method of fault detection and classification was presented in [7] for power transmission

lines based on convolutional sparse autoencoder. A robust fault detection and discrimination technique for transmission lines was proposed in [8], which utilizes a robust method of phasor estimation to compute accurate fault impedance along with a feature value extracted from the samples of voltage and current signals. A new algorithm was introduced in [9] for short-circuit fault detection and identification based on state estimation taking into account the measurements in active distribution systems.

In contrast to the aforementioned references, this paper provides a different method by using SHS. Within the SHS framework, this paper is focused on exploring the potential of using common sensors such as PMUs or frequency or voltage for detecting contingency and estimating internal states jointly, for enhancing reliability and expanding the capability of contingency detection. To the best of our knowledge, this paper is the first effort in applying the SHS to detect contingencies in power systems. Our approach is based on the theoretical foundation of our recent papers [10], [11]. It should be emphasized that as a newly developed theoretical work, applications of the results from [10], [11] in power systems are highly challenging, including derivation of virtual dynamic SHS models, their linearization, algorithm implementation, and convergence validation, etc. By using collaboratively dynamic hybrid system models, stochastic information on system jumps, and advanced observer design methods, this paper achieves contingency detection and state estimation simultaneously.

The main contributions of this paper are summarized as follows:

- 1) It introduces an approach of using SHS for joint contingency detection and state estimation. The interwinding nature of continuous state and switching processes makes it necessary to perform joint estimation for contingency detection. By employing the rich information from the dynamic system models, it becomes possible to jointly detect contingencies and estimate the continuous states by using only limited numbers of sensors. The joint estimation problem is much more complicated than the state estimation problems in power systems since they assume the dynamic system is known.
- 2) It introduces a design method for selecting an input probing such that contingencies of different types and locations can be detected by using only a limited set of sensors. A mode-modulated input design method for suitably selecting inputs is presented so that detectability on contingencies can be persistently sustained.
- 3) It develops a two-time-scale framework and algorithms for jointly detecting contingencies and estimating the continuous states simultaneously. Convergence properties of the algorithms are established.
- 4) It employs two common IEEE testing systems to validate and evaluate models, detection algorithms, observer design, convergence properties, and algorithm robustness. The methods of this paper are highly scalable. The complexity of the virtual dynamic SHS depends on the number of dynamic buses that can be numerically derived using commercial software packages of power

flow analysis such as MATPOWER. These numerical methods have been used in case studies on the IEEE 33-bus system.

The paper is organized as follows. Section II defines notations and the main problems of this paper. Section III derives state space models of MGs. Sensor systems, contingencies, and stochastic hybrid systems are described in Section IV. Section V presents observer design procedures and detection algorithms, and establishes convergence. Performance evaluation case studies are discussed in Section VI. The main conclusions of this paper are summarized in Section VII.

II. PRELIMINARIES

For a column vector $v \in \mathbb{R}^n$, $\|v\|$ is its Euclidean norm. For a matrix $M \in \mathbb{R}^{n \times m}$, M^\top is its transpose, $\lambda(M)$ is an eigenvalue of M , and $\sigma(M) = \sqrt{\lambda(M^\top M)}$ is a singular value of M . The kernel or null space of $M \in \mathbb{R}^{n \times m}$ is $\ker(M) = \{x \in \mathbb{R}^m : Mx = 0\}$ and its range is $\text{Range}(M) = \{y = Mx : x \in \mathbb{R}^m\}$. For a subspace $\mathbb{U} \subseteq \mathbb{R}^n$ of dimension p , a matrix $M \in \mathbb{R}^{n \times p}$ is said to be a base matrix of \mathbb{U} , written as $M = \text{Base}(\mathbb{U})$, if the column vectors of M are linearly independent and $\text{Range}(M) = \mathbb{U}$. A function $y(t) \in \mathbb{R}$ in a time interval $[0, \tau)$ is piecewise continuously differentiable if $[0, \tau)$ can be divided into a finite number of subintervals $[t_{k-1}, t_k)$, $k = 1, \dots, \ell$, $t_0 = 0$, $t_\ell = \tau$ such that $y(t)$ is right continuous in $[t_{k-1}, t_k)$ and continuously differentiable, to any order as needed, in (t_{k-1}, t_k) . The space of such functions is denoted by $\mathcal{C}[0, \tau)$.

For an AC power microgrid, all voltages and currents will be represented by their phasors $\vec{V} = V\angle\delta$ and $\vec{I} = I\angle\gamma$. Sensors in power systems are highly diversified, including PMUs, frequency, voltage, power measurements, signal transducers for protection, rotational speed, torque, temperature, among many others. Furthermore, communication systems are used for data transmission. The microgrid can be viewed as a networked system with γ buses connected by transmission lines. This network system is represented by a graph $\mathcal{N} = \{\mathcal{V}, \mathcal{E}\}$ where \mathcal{V} is the set of buses (vertices in a graph) and \mathcal{E} is the set of feeder/transmission links (edges in a graph). The transmission line $(i, j) \in \mathcal{E}$ is bi-directional, i.e., $(i, j) \in \mathcal{E} \rightarrow (j, i) \in \mathcal{E}$. For Bus i , its neighbor \mathcal{N}_i is the set of buses j that are connected to it, namely, $\mathcal{N}_i = \{j \in \mathcal{V} : (i, j) \in \mathcal{E} \text{ or } (j, i) \in \mathcal{E}\}$. By default, $(i, i) \in \mathcal{E}$.

III. STATE SPACE MODELS OF MICROGRIDS

We now summarize the main SHS framework introduced and detailed in [5]. We should emphasize that the framework is highly general. For demonstration, we will use real power management problems in case studies. Power systems are highly complicated and interconnected systems. Microgrids are unique in which power generations can step from traditional synchronous generators, power-electronics-based wind turns, solar panels, battery systems, and controllable loads. To derive a state space model representation of SHS of power systems, it is essential to characterize bus types according to their dynamics. Consequently, we divide buses into two types: dynamic buses and non-dynamic buses. This classification is

independent of traditional classifications such as PV/PQ buses or dispatchable/non-dispatchable buses.

A. Dynamic Buses

If Bus i is dynamic, then it is represented by a local state space model,

$$\dot{z}_i^d = f_i(z_i^d, z_i^-, v_i^d, \ell_i^d), \quad (1)$$

where z_i^d is the local state variable, z_i^- is the neighboring variables of Bus i which may be state variables of its neighboring dynamic buses, or intermediate variables of its neighboring non-dynamic buses, v_i^d is the local control input, and ℓ_i^d is the local congregated total load that cannot be actively controlled, such as regular loads, fixed-blade wind generators, solar panels, constant-charging-current batteries, etc. The control input is set of controllable (i.e., dispatchable) variables such as generator mechanical power input, controllable loads, actively managed battery systems, tunable wind turbines, etc. If a bus does not have any dispatchable assets, then $v_i^d = 0$.

B. Non-dynamic Buses

If the j th bus is non-dynamic, which is in a steady state or pseudo-steady state, then it is represented by an implicit algebraic relationship,

$$0 = g_j(z_j^{nd}, z_j^-, v_j^{nd}, \ell_j^{nd}), \quad (2)$$

where z_j^{nd} is the local state variable vector, z_j^- is the neighboring variables, v_j^{nd} is the local control input, and ℓ_j^{nd} is the local load.

Remark 1:

- 1) Dynamic/non-dynamic designation is related to the local system's models. They do not affect the designation of power flow analysis such as PV, PQ, slack buses. For example, a load is typically considered as a PQ bus. If the load is motor with its own dynamic model, then the bus is a dynamic bus.
- 2) Traditionally, generators are dynamic. But fast reaction power sources like batteries, may be simplified as non-dynamic and represented by their near-steady-state algebraic relationships. For the same token, loads can be either static (non-dynamic) or dynamic. The ZIP and exponential load models are static. But induction motors are usually modeled dynamic systems, and so are exponential recovery load (ERL) models.
- 3) Dynamic/non-dynamic bus classification can change when local sensors and controllers are included. For example, PID controllers are dynamic systems and after applying them to control a non-dynamic system on a bus, the bus becomes dynamic.
- 4) Dynamic/non-dynamic designation also does not affect whether a bus is dispatchable or not. A dispatchable resource has controllable real or reactive powers to participate in control or market of a power grid. It is represented as part of the control input v_i^d in (1).

The general nonlinear state equation (1) is highly versatile in representing dynamic systems on a bus. For example, this may be a common swing equation for synchronous generators

$$M_i \dot{\omega}_i + g_i(\omega_i) = P_i^{in} - P_i^L - P_i^{out}, \quad (3)$$

where δ_i is its electric angle, $\omega_i = \dot{\delta}_i$, M_i is the equivalent electric-side inertia, $g_i(\cdot)$ represents the nonlinear damping effect, and $g_i(\cdot)$ is continuously differentiable satisfying $\omega_i g_i(\omega_i) > 0$ for $\omega_i \neq 0$. Linearization of $g_i(\cdot)$ around $\omega_i = 0$ is $b_i \omega_i$ with $b_i > 0$. Also, P_i^{out} is the total transmitted power from Bus i to its neighboring buses. As an extension, if it is required to include steam turbine control with generators, the dynamic model will combine both turbine and generator dynamics and state variables will then include flow rate and other mechanical system variables. However, if a bus has a renewable generator or a battery system with power electronic based control mechanisms, then their dynamic models will be different, inherited from the specific dynamic models derived for such physical systems.

For both dynamic and non-dynamic buses, the interaction of the local variables with their neighboring buses is based on the standard power flow relationships. Suppose that the transmission line between Bus i and Bus j has impedance $X_{ij} \angle \theta_{ij}$. The line current is

$$I_{ij} \angle \gamma = \frac{V_i \angle \delta_i - V_j \angle \delta_j}{X_{ij} \angle \theta_{ij}} = \frac{V_i}{X_{ij}} \angle (\delta_i - \theta_{ij}) - \frac{V_j}{X_{ij}} \angle (\delta_j - \theta_{ij}).$$

Denote $\delta_{ij} = \delta_i - \delta_j$. The complex power flow from Bus i to Bus j at Bus i is

$$S_{ij} = V_i \angle \delta_i \times I_{ij} \angle (-\gamma) = \frac{V_i^2}{X_{ij}} \angle \theta_{ij} - \frac{V_i V_j}{X_{ij}} \angle (\theta_{ij} + \delta_{ij}),$$

which implies that the transmitted real and reactive powers at Bus i are

$$P_{ij} = \frac{V_i^2}{X_{ij}} \cos(\theta_{ij}) - \frac{V_i V_j}{X_{ij}} \cos(\theta_{ij} + \delta_{ij}),$$

$$Q_{ij} = \frac{V_i^2}{X_{ij}} \sin(\theta_{ij}) - \frac{V_i V_j}{X_{ij}} \sin(\theta_{ij} + \delta_{ij}).$$

C. Virtual Dynamic State Space Models

Suppose that the γ buses in \mathcal{N} contain γ^d dynamic buses and $\gamma^{nd} = \gamma - \gamma^d$ non-dynamic buses.¹ Without loss of generality, let the first γ^d buses be dynamic. Define the states, inputs, loads of dynamic buses and non-dynamic buses as

$$z^d = \begin{bmatrix} z_1^d \\ \vdots \\ z_{\gamma^d}^d \end{bmatrix}, v^d = \begin{bmatrix} v_1^d \\ \vdots \\ v_{\gamma^d}^d \end{bmatrix}, \ell^d = \begin{bmatrix} \ell_1^d \\ \vdots \\ \ell_{\gamma^d}^d \end{bmatrix}$$

and

$$z^{nd} = \begin{bmatrix} z_{\gamma^d+1}^{nd} \\ \vdots \\ z_{\gamma}^{nd} \end{bmatrix}, v^{nd} = \begin{bmatrix} v_{\gamma^d+1}^{nd} \\ \vdots \\ v_{\gamma}^{nd} \end{bmatrix}, \ell^{nd} = \begin{bmatrix} \ell_{\gamma^d+1}^{nd} \\ \vdots \\ \ell_{\gamma}^{nd} \end{bmatrix}.$$

Define the state, input, and load of all buses as $z = \begin{bmatrix} z^d \\ z^{nd} \end{bmatrix}$, $v = \begin{bmatrix} v^d \\ v^{nd} \end{bmatrix}$, $\ell = \begin{bmatrix} \ell^d \\ \ell^{nd} \end{bmatrix}$. By (2), for non-dynamic buses, we have

$$G^0(z^{nd}, z^d, v^{nd}, \ell^{nd}) = \begin{bmatrix} g_{\gamma^d+1}(z_{\gamma^d+1}^{nd}, z_{\gamma^d+1}^-, v_{\gamma^d+1}^{nd}, \ell_{\gamma^d+1}^{nd}) \\ \vdots \\ g_{\gamma}(z_{\gamma}^{nd}, z_{\gamma}^-, v_{\gamma}^{nd}, \ell_{\gamma}^{nd}) \end{bmatrix} = 0.$$

¹Since this paper deals with state estimation under state space models, we assume that $1 \leq \gamma^d \leq \gamma$, namely at least one bus is dynamics. But $\gamma^{nd} = 0$ is possible, meaning that all buses are dynamic.

For physical power grids, given z^d, v^{nd}, ℓ^{nd} , this equation has a unique solution within permitted operating ranges, leading to the symbolic relationship $z^{nd} = H(z^d, v^{nd}, \ell^{nd})$. Furthermore, by the dynamic systems in (2), $\dot{z}^d = F^0(z^d, z^{nd}, v^d, \ell^d)$. Then, we obtain

$$\dot{z}^d = F^0(z^d, H(z^d, v^{nd}, \ell^{nd}), v^d, \ell^d) = F(z^d, v^d, v^{nd}, \ell^d, \ell^{nd}). \quad (4)$$

D. Linearization

In power system control problems, it is common to linearize the nonlinear dynamics (4) near nominal operating points [1], [12]. The linearization process involves the following standard steps. Given the steady-state loads $\bar{\ell} = [\bar{\ell}^d, \bar{\ell}^{nd}]^\top$ and steady-state input real powers $\bar{v} = [\bar{v}^d, \bar{v}^{nd}]^\top$, the steady-state \bar{z}^d (equilibrium point or the nominal operating condition) is the solution to $F(\bar{z}^d, \bar{v}^d, \bar{v}^{nd}, \bar{\ell}^d, \bar{\ell}^{nd}) = 0$.

By defining the perturbation variables from their nominal values as $x = z^d - \bar{z}^d, u = v^d - \bar{v}^d, u^n = v^{nd} - \bar{v}^{nd}, \zeta = \ell^d - \bar{\ell}^d, \zeta^n = \ell^{nd} - \bar{\ell}^{nd}$, the linearized system is

$$\dot{x} = Ax + B_1u + B_2u^n + D_1\zeta + D_2\zeta^n, \quad (5)$$

where the matrices are the related Jacobian matrices $A = \frac{\partial F(\cdot)}{\partial z^d}, B_1 = \frac{\partial F(\cdot)}{\partial v^d}, B_2 = \frac{\partial F(\cdot)}{\partial v^{nd}}, D_1 = \frac{\partial F(\cdot)}{\partial \ell^d}, D_2 = \frac{\partial F(\cdot)}{\partial \ell^{nd}}$ at $z^d = \bar{z}^d, v = \bar{v}, \ell = \bar{\ell}$.

Example 1: Suppose that the generators can be represented by the swing equations

$$M_i \dot{\omega}_i + g_i(\omega_i) = P_i^{in} - P_i^L - P_i^{out},$$

where δ_i is its electric angle, $\omega_i = \dot{\delta}_i$, M_i is the equivalent electric-side inertia, $g_i(\cdot)$ represents the nonlinear damping effect, and $g_i(\cdot)$ is continuously differentiable satisfying $\omega_i g_i(\omega_i) > 0$ for $\omega_i \neq 0$. Linearization of $g_i(\cdot)$ around $\omega_i = 0$ is $b_i \omega_i$ with $b_i > 0$. Also, P_i^{out} is the total transmitted power from Bus i to its neighboring buses, i.e., $P_i^{out} = \sum_{j \in \mathcal{N}_i} P_{ij} = \sum_{j \in \mathcal{N}_i} \left[\frac{V_i^2}{X_{ij}} \cos(\theta_{ij}) - \frac{V_i V_j}{X_{ij}} \cos(\theta_{ij} + \delta_{ij}) \right] = \sum_{j \in \mathcal{N}_i} q(\delta_i, \delta_j)$, where $q(\delta_i, \delta_j) = \frac{V_i^2}{X_{ij}} \cos(\theta_{ij}) - \frac{V_i V_j}{X_{ij}} \cos(\theta_{ij} + \delta_{ij})$. The two-bus system shown in Fig. 1 has $\theta_{12} = 90^\circ$ which is the angle of impedance, namely the transmission line is lossless. Both buses are dynamic dispatchable buses with state variables $z_1^d = [\delta_1; \omega_1], z_2^d = [\delta_2; \omega_2]$. Suppose that $g_1(\omega_1) = b_1 \omega_1$, $b_1 > 0$, and $g_2(\omega_2) = b_2 \omega_2$, $b_2 > 0$. Denote $\beta = \beta_{12} = V_1 V_2 / X_{12}$ and $\delta = \delta_1 - \delta_2$. Then, $f_1(z_1^d, z_2^d) = \left[\omega_1; -\frac{b_1 \omega_1}{M_1} - \frac{1}{M_1} \beta \sin(\delta) \right], f_2(z_2^d, z_1^d) = \left[\omega_2; -\frac{b_2 \omega_2}{M_2} - \frac{1}{M_2} \beta \sin(-\delta) \right]$

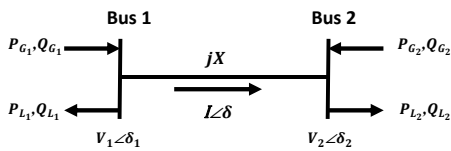


Fig. 1. A link in microgrids

Given $\bar{v}_1 = P_1^{in}, \bar{v}_2 = P_2^{in}, \bar{\ell}_1 = P_1^L, \bar{\ell}_2 = P_2^L$, the equilibrium point is $\bar{\omega}_1 = 0, \bar{\omega}_2 = 0$, and $\bar{\delta} = \sin^{-1} \left(\frac{P_1^{in} - P_1^L}{\beta} \right)$.

Assume $M_1 = 1, M_2 = 1.5, b_1 = 0.2, b_2 = 0.31, \beta = 200, P_1^{in} = 100, P_2^{in} = 50, P_1^L = 70, P_2^L = 80$. Then, the equilibrium point is $\bar{\delta} = 0.1506$ (rad). Under these given values, the linearized system is (5) with

$$A = \begin{bmatrix} 0 & 1 & 0 & 0 \\ -197.7372 & -0.2 & 197.7372 & 0 \\ 0 & 0 & 0 & 1 \\ 131.8248 & 0 & -131.8248 & -0.2067 \end{bmatrix}, \quad (6)$$

$$B_1 = \begin{bmatrix} 0 & 0 \\ 1/M_1 & 0 \\ 0 & 0 \\ 0 & 1/M_2 \end{bmatrix}, \quad D_1 = \begin{bmatrix} 0 & 0 \\ -1/M_1 & 0 \\ 0 & 0 \\ 0 & -1/M_2 \end{bmatrix}, \quad B_2 = 0, \quad D_2 = 0.$$

IV. CONTINGENCIES AND STOCHASTIC HYBRID SYSTEM MODELS

A. Sensor Systems and Observability

For power system operation and contingency detection, many sensors must be deployed, such as voltages, frequencies, PMUs, over-current protection transducers, among many others. Sensor selection and placement are important for managing SHS. Mathematically, sensor choice (which variable to measure) and location (which bus to measure) are reflected in the output equation (5).

Adding a sensor system with $y = Cx$ where C is the sensing matrix, we have the following state space model:

$$\begin{cases} \dot{x} = Ax + B_1u + B_2u^n + D_1\zeta + D_2\zeta^n, \\ y = Cx. \end{cases} \quad (7)$$

Remark 2: The system (7) is a linearized system whose variables are perturbations from their nominal values. Physically, y is the difference between the measured value y_{measured} and the nominal value y_{nominal} at the operating point. For example, the phasors on buses can be measured by PMUs. Suppose that only δ_1 is measured, this can be represented by $y = \delta_1 - \bar{\delta}_1 = C_1x$, with $C_1 = [1, 0, 0, 0]$. It is easy to verify that under this observation equation, the system is observable. On the other hand, the measurement of the real power $P_{12} = \beta \sin(\delta) = \beta \sin(\delta_1 - \delta_2)$ can be represented as $y = C_2x$, with $C_2 = [\beta \cos(\bar{\delta}), 0, -\beta \cos(\bar{\delta}), 0]$. Different sensor systems affect observability, which characterizes if the measured values are sufficient to determine the interval (unmeasured) states. Under the system parameters in *Example 1*, if we measure the power transfer P_{12} with $y = C_2x$ the observability matrix is

$$W_2 = \begin{bmatrix} 1 & 0 & -1 & 0 \\ 0 & 1 & 0 & -1 \\ -329.5620 & -0.2 & 329.5620 & 0.2067 \\ 66.7912 & -329.5220 & -66.7912 & 329.5193 \end{bmatrix},$$

which has rank 3. As a result, this state space model is not observable in this case.

B. Contingency Models

Power system contingencies are of diversified types. We list some of the common types.

- 1) **Transmission Line Grounding:** A transmission line fault can change the impedance values $|Z|$ on the line.

For example, a single-phase grounding will reduce the impedance value. In contrast, high-impedance faults are very common in case of single-phase faults. Since line impedances are parameters in the matrix A , a line fault will cause a jump in the A matrix value.

- 2) **Transmission Line Breaking:** When a transmission line breaks due to natural disasters or faulty components, the transmission line's impedance will experience a jump of X_{ij} to a much bigger value;
- 3) **Generator Excitation System Fault:** Loss of excitation (LOE) is a common fault in generators. LOE causes a sudden decline of the terminal voltage V , with some other potential damages to the generator.
- 4) **Intentional Attack:** Cyber attackers may intentionally damage a sensor, a transmission line, a bus, creating a jump in system structure or parameters.

Traditionally, contingencies are detected by special devices that monitor the targeted buses and lines. For example, impedance relays are very common devices for protecting high-voltage transmission lines from faults. This paper introduces SHS models for contingency detection. Under this framework and our algorithms, a PMU on one bus can potentially detect impedance jumps of many lines without using special devices on these lines. This will be demonstrated in the case studies.

Power system contingencies can be generally modeled as jumps on system matrices. Mathematically, we list all scenarios of contingencies under study as a set $\mathcal{S} = \{1, \dots, m\}$ and use a jumping process $\alpha(t) \in \mathcal{S}$ to represent the occurrence of the corresponding scenario. For example, for the system in (6), the above-listed faults are reflected on the coefficient $\beta = V_1 V_2 / X_{12}$ as a switching of its value during contingency. If the excitation system for Bus 1 experiences a loss-of-magnet fault on its excitor, then V_1 will drop. On the other hand, a partial transmission line fault, such as a one-phase line grounding, changes the impedance value X_{12} , leading to a jump in β value. Suppose that β changes its value from 200 to 100. Then, the new $\bar{\delta}$ value is $\bar{\delta}_2 = 0.3047$ and the system's matrix becomes the following new one:

$$A_2 = \begin{bmatrix} 0 & 1 & 0 & 0 \\ -190.7878 & -0.2 & 190.7878 & 0 \\ 0 & 0 & 0 & 1 \\ 127.1919 & 0 & -127.1919 & -0.2067 \end{bmatrix}.$$

C. Randomly Switched Linear Systems

The dependence of system matrices on contingencies can be represented by their values as functions of α , expressed as $A(\alpha)$, $B_1(\alpha)$, $B_2(\alpha)$, $D_1(\alpha)$, $D_2(\alpha)$ and $C(\alpha)$. Since contingencies occur randomly, $\alpha(t)$ is a stochastic process. Including the jumping process into the system dynamics (7) introduces the following hybrid system:

$$\begin{cases} \dot{x} = A(\alpha)x + B_1(\alpha)u + B_2(\alpha)u^n + D_1(\alpha)\zeta + D_2(\alpha)\zeta^n, \\ y = C(\alpha)x. \end{cases} \quad (8)$$

This system is an RSLs. The contingency detection problem aims to study joint discrete event detection and continuous state estimation of RSLs.

The system matrices depend on the randomly switching process $\alpha(t)$ that takes m possible values in a discrete state space $\mathcal{S} = \{1, \dots, m\}$. For each given value $i \in \mathcal{S}$, the corresponding linear time invariant (LTI) system in (8) with matrices $(C(i), A(i), B_1(i), B_2(i), D_1(i), D_2(i))$ is called *the i th subsystem* of the RSLs. We introduce the following assumptions on the random switching process for the theoretical analysis.

Assumption 1: Given a sampling interval τ , (i) the switching process $\alpha(t)$ can switch only at the instants $k\tau$, $k = 0, 1, 2, \dots$, that generates a stochastic sequence $\{\alpha_k = \alpha(k\tau)\}$ (*the skeleton sequence*); (ii) The sequence $\{\alpha_k\}$ is independent and identically distributed (i.i.d.) with probability $\Pr\{\alpha_k = i\} = p_i > 0$, $i \in \mathcal{S}$, and $\sum_{i=1}^m p_i = 1$; (iii) α_k is independent of $x(0)$ and the Brownian motion w .

The main difference of *Assumption 1* from [5] is that $\alpha(t)$ cannot be directly measured and must be estimated here in this paper. Note also that power system management usually imposes certain intervals for data processing. For example, PMU data rate of the Power Xpert Meter is 1024 samples per cycle. For contingency management, 160 ms is the IEEE imposed limit for voltage sag/surge. For slower dynamics of power dispatch, a decision interval of 5 minutes is commonly used in practice. Mathematically, under this assumption, the random switching process can be treated as a discrete-time stochastic sequence, rather than a continuous-time process.

Under *Assumption 1*, $A_k = A(\alpha_k) = \sum_{i=1}^m A(i) \mathbb{1}_{\{\alpha_k=i\}}$, $B_k^1 = B_1(\alpha_k) = \sum_{i=1}^m B_1(i) \mathbb{1}_{\{\alpha_k=i\}}$, $B_k^2 = B_2(\alpha_k) = \sum_{i=1}^m B_2(i) \mathbb{1}_{\{\alpha_k=i\}}$, $C_k = C(\alpha_k) = \sum_{i=1}^m C(i) \mathbb{1}_{\{\alpha_k=i\}}$, where $\mathbb{1}_G$ is the indicator function of the event G : $\mathbb{1}_G = 1$ if G is true; and $\mathbb{1}_G = 0$, otherwise. These are matrix-valued random variables. The sampled values of the signals are denoted by $x_k = x(k\tau)$, $y_k = y(k\tau)$.

The premise of this paper is to treat RSLs whose initial states are unknown and whose switching sequence α_k cannot be directly measured. As a result, both the continuous state x_k and discrete state α_k must be estimated from the known input $u(t)$ and the observed output $y(t)$. The available data set in a time interval $[0, \tau)$ is given by the noise-free data set $\mathcal{D}_\tau = \{y(t), t \in [0, \tau)\}$ for a given $\tau > 0$.

D. State Space Decomposition

For the i th subsystem in \mathcal{S} , $A(i)$ and $C(i)$ are constant matrices, and its observability matrix is $W(i) = \begin{bmatrix} C(i) \\ C(i)A(i) \\ \vdots \\ C(i)(A(i))^{n-1} \end{bmatrix}$. Denote $W_{\mathcal{S}} = \begin{bmatrix} W(1) \\ \vdots \\ W(m) \end{bmatrix}$ as the combined observability matrix for \mathcal{S} . We note that both $W(i)$ and $W_{\mathcal{S}}$ are deterministic matrices that contain only information on subsystems. They do not involve actual switching sequences. Thus, they can be evaluated off-line.

Assumption 2: (i) Subsystems may be unobservable, namely, $\text{Rank}(W(i)) = n_i \leq n$, $i \in \mathcal{S}$; (ii) $W_{\mathcal{S}}$ is full column rank.

By *Assumption 2*, since the i th subsystem may be unobservable, namely, $\text{Rank}(W(i)) = n_i < n$, we construct $M_i = \text{Base}(\ker(W(i))) \in \mathbb{R}^{n \times (n-n_i)}$ and select any $N_i \in \mathbb{R}^{n \times n_i}$

such that $T_i = [M_i, N_i]$ is invertible. The inverse of T_i is decomposed into $T_i^{-1} = \begin{bmatrix} K_i \\ F_i \end{bmatrix}$, where $K_i \in \mathbb{R}^{(n-n_i) \times n}$ and $F_i \in \mathbb{R}^{n_i \times n}$.

The state transformation $\tilde{z}^i = T_i^{-1}x$ can be decomposed into $\tilde{z}^i = T_i^{-1}x = \begin{bmatrix} K_i x \\ F_i x \end{bmatrix} = \begin{bmatrix} v^i \\ z^i \end{bmatrix}$ where $z^i \in \mathbb{R}^{n_i}$. Correspondingly, this coordinate transformation leads to the transformed matrices $A^i = T_i^{-1}A(i)T_i$, $B^i = T_i^{-1}B(i)$, $C^i = C(i)T_i$, with the structures $A^i = \begin{bmatrix} A_{11}^i & A_{12}^i \\ 0 & A_{22}^i \end{bmatrix}$, $B^i = \begin{bmatrix} B_1^i \\ B_2^i \end{bmatrix}$, $C^i = [0, C_2^i]$ with $A_{22}^i \in \mathbb{R}^{n_i \times n_i}$ and $C_2^i \in \mathbb{R}^{1 \times n_i}$. As a result, if we focus only on the dynamics of the observable partial state z^i , we have

$$\begin{cases} \dot{z}^i &= A_{22}^i z^i + B_2^i u, \\ y &= C_2^i z^i, \end{cases} \quad (9)$$

where (C_2^i, A_{22}^i) is observable.

V. CONTINGENCY DETECTION

Under our stochastic hybrid system models, contingencies are represented by jumps in system structures and parameters. Mathematically, they are indexed by the stochastic process α_k . Consequently, contingency detection in power systems becomes a problem of estimating α_k correctly when it jumps, on the basis of output observations. At $t = k\tau$, the internal continuous state $x_k = x(k\tau)$ is also unknown and must be estimated from the same output y . As a result, we must develop reliable joint estimation algorithms for estimating both α_k and x_k simultaneously.

This joint estimation problem in power systems encounters many challenging issues, including detectability, joint estimation algorithms, convergence, and reliability. For instance, power systems are complicated network systems. In the $N-1$ reliability standard of power systems, one considers a fault on one transmission line, with other transmission lines under normal operating conditions. It will be shown in our case studies that the resulting system matrices $A(i)$ will typically share common eigenvalues since only a small part of the grid has changed its parameter values. In our recent theoretical work [11], it has been shown that without using input assistance, the stochastic hybrid system is not detectable, namely, some contingencies cannot be detected by the existing sensor systems.

Due to this complication, to ensure the ability to detect contingencies, it is necessary to add a small probing input u . When the input is applied to an unknown subsystem with unknown initial state, the output contains both the input response and initial-state response. Input design and contingency detection algorithms are critical in this complicated situation.

A. Input Design Principles

First, we demonstrate by a simple example that the input must be suitably designed. Otherwise, even with input assistance, contingency detection may not be achievable.

Example 2: Consider an RLS with two subsystems: $A(1) = \begin{bmatrix} -4 & 0 \\ 0 & -5 \end{bmatrix}$, $B(1) = \begin{bmatrix} 1 \\ 1 \end{bmatrix}$, $C(1) = [1 \ 1]$; $A(2) =$

$\begin{bmatrix} -4 & 0 \\ 0 & -10 \end{bmatrix}$, $B(2) = \begin{bmatrix} 1 \\ 1 \end{bmatrix}$, $C(2) = [1 \ 2]$. We need to detect $\alpha_k \in \{1, 2\}$ by using the output measurement data.

We first note that these two subsystems have the same eigenvalue -4 , so they cannot be distinguished without assistance from a probing input. Suppose that we use the unit step $U(s) = 1/s$ as the input signal. Then the two subsystems have respective transfer functions $G_1(s) = \frac{1}{s+4} + \frac{1}{s+5} = \frac{2s+9}{(s+4)(s+5)} \in \mathcal{R}$; $G_2(s) = \frac{1}{s+4} + \frac{2}{s+10} = \frac{3s+18}{(s+4)(s+10)} \in \mathcal{R}$. Their total respective responses to the input and (unknown) initial state are

$$\begin{aligned} y_1(t) &= a_1 e^{-4t} + a_2 e^{-5t} + 9/20 - (1/4)e^{-4t} - (1/5)e^{-5t}, \\ y_2(t) &= b_1 e^{-4t} + b_2 e^{-10t} + 9/20 - (1/4)e^{-4t} - (1/5)e^{-10t}, \end{aligned}$$

for $t \in [0, \tau)$, where a_1, a_2, b_1, b_2 are determined by the initial states. Denote their difference as

$$\begin{aligned} \delta(t) &= y_1(t) - y_2(t) \\ &= (a_1 - b_1)e^{-4t} + (a_2 - 1/5)e^{-5t} + (b_2 - 1/5)e^{-10t}. \end{aligned}$$

Then, the difference becomes $\delta(t) \equiv 0, t \in [0, \tau)$ if $a_1 = b_1, a_2 = 1/5, b_2 = 1/5$. In other words, we cannot uniquely determine if the subsystem is $\alpha_k = 1$ or $\alpha_k = 2$ in this case.

The theoretical foundation of this method was introduced in [11] and is summarized below. As a first-time introduction of this method into power system contingency detection, some algorithm details are added and important related features of power system dynamic models and their impact on contingency detection are highlighted in the following part.

Example 2 indicates that the input signal must be suitably designed to enhance detectability on contingencies, and some design principles must be followed in selecting suitable inputs for contingency detection. Consider the set $G = \{G_i, i = 1, \dots, m\}$ of m distinct subsystems. The set of poles of G_i (or equivalently the eigenvalues of $A(i)$) is Λ_i and $\Lambda = \cup_{i=1}^m \Lambda_i$.

Assumption 3: Let $\mathcal{U} \subset \mathcal{R}_0$ be the set of non-vanishing inputs u whose Laplace transforms $U(s)$ satisfy the following conditions: (i) $U(s) = \frac{b(s)}{a(s)}$ is coprime, namely, no common pole-zero pairs (i.e., no pole-zero cancellation); (ii) $U(s)$ contains at least one pole λ of any multiplicity $q \geq 1$ such that $\lambda \notin \Lambda$ and $G_i(\lambda), i = 1, \dots, m$, are distinct.

The following result from [11] forms the foundation for the input design.

Theorem 1: [11] For the set of distinct subsystems $G = \{G_i, i = 1, \dots, m\}$, if the input $u \in \mathcal{U}$, where \mathcal{U} is given in *Assumption 3*, then for any $\tau > 0$, the true subsystem can be uniquely determined from the data set $\mathcal{D}_\tau = \{y(t) \neq 0, t \in [0, \tau)\}$, regardless of the actual initial state $x(0)$.

B. Two-Time-Scale Framework and Joint Estimation Algorithms

The contingency detection and continuous-state observers will be implemented in a two-time-scale framework. Each time segment $[k\tau, (k+1)\tau)$ is divided into two intervals. The first smaller interval $[k\tau, k\tau + \tau_0)$ is designated for estimating α_k (that is, identifying the active subsystem). During this time interval, the probing input u that satisfies the conditions of *Theorem 1* is applied to assist in determination of α_k . Once $\alpha_k = i$ is correctly estimated, in the second interval $[k\tau + \tau_0, (k+1)\tau)$, a feedback-based observer is implemented for the i th subsystem to estimate its observable sub-state z^i .

1) *Detection of α_k using Data in $[k\tau, k\tau + \tau_0]$* : α_k is detected by the following algorithm.

Algorithm 1 Detection of α_k under Unknown Initial State

- 1: Calculate the eigenvalues of all $A(i)$ and denote as Λ . Take u satisfying Assumption 3 as the designed input.
 - 2: Under the designed input u , collect and sample the output data on $y(t)$ in $[k\tau, k\tau + \tau_0]$. Define a small sampling interval t_s : Let $N_0 = \tau_0/t_s$ be an integer. Obtain sampled values $y(k\tau + \ell t_s)$, $\ell = 0, \dots, N_0$.
 - 3: Compute the input responses of the subsystems (assuming zero initial condition): $y_i^{input}(\ell) = (G_i u)(k\tau + \ell t_s)$, $\ell = 0, \dots, N_0$. Since the input u and the system transfer functions G_i are known in advance, these responses can be computed offline and stored.
 - 4: Derive the net initial state responses of the subsystems: $y_i^{net}(\ell) = y(k\tau + \ell t_s) - y_i^{input}(\ell)$, $\ell = 0, \dots, N_0$.
 - 5: Estimating the initial observable sub-states of the subsystems: Derive the numerical Gramians of the subsystems $\Gamma_i = \sum_{\ell=0}^{N_0} t_s e^{A(i)\ell t_s} C^T(i) C(i) e^{A(i)\ell t_s}$ and $Y_i = \sum_{\ell=0}^{N_0} t_s e^{A(i)\ell t_s} C^T(i) y_i^{net}(\ell)$. Then, $\hat{x}_k^i = \Gamma_i^{-1} Y_i$.
 - 6: Calculate the total estimated outputs of the subsystems: $\hat{y}_i(\ell) = C(i) e^{A(i)\ell t_s} \hat{x}_k^i + y_i^{input}(\ell)$.
 - 7: Calculate the output prediction errors of the subsystems $\varepsilon_i = \frac{1}{N_0+1} \sum_{\ell=0}^{N_0} |\hat{y}_i(\ell) - y(k\tau + \ell t_s)|$. This error measure may be replaced by the common Euclidean norm or the max norm.
 - 8: Determine α_k : $\hat{\alpha}_k = \arg \min_{i=1, \dots, m} \varepsilon_i$.
-

2) *Observer Design for x in $[k\tau + \tau_0, (k+1)\tau]$* : After determining $\alpha_k = i$ correctly, an observer can be designed to estimate $z^i(k\tau + \tau_0)$. The errors in estimating z^i and z are denoted by $e_i = z^i - \hat{z}^i$ and $e = z - \hat{z}$, respectively. Denote $\mu^i(t) = \|e_i(t)\|$, $\mu_k^i = \|e_i(k\tau)\|$, $\mu(t) = \|e(t)\|$, $\mu_k = \|e(k\tau)\|$.

Assumption 4: We assume that (i) The RSLs has independent subspace error dynamics, namely \dot{z}^i depends on z^i only, independent of α_k , under zero input. For such systems, the *subsystem state equation* will be $\dot{e}_i = A_{22}^i e_i$ in open loop without input; (ii) B_k is known.

Under *Assumption 4*, we consider the following three cases in the error analysis:

Case 1: $t \in [k\tau, k\tau + \tau_0]$

In this time interval, all subsystem observers are running open-loop. Since a probing input is applied, under *Assumption 4*, the dynamics of z^i are $\dot{z}^i = F_i \dot{x} = F_i A_k x + F_i B_k u = A_{22}^i z^i + F_i B_k u$. The observer is $\dot{\hat{z}}^i = A_{22}^i \hat{z}^i + F_i B_k u$. It follows that the error dynamics are $\dot{e}_i = A_{22}^i e_i$, and $\|e_i(k\tau + \tau_0)\| \leq \gamma_0^i$, for some $\gamma_0^i > 0$. Let $\gamma_0 = \max_{i=1, \dots, m} \gamma_0^i$.

Case 2: $t \in [k\tau + \tau_0, (k+1)\tau]$ and $\alpha_k \neq i$

In the interval $t \in [k\tau + \tau_0, (k+1)\tau]$, the input $u \equiv 0$. When the i th subsystem is running open loop, we have the error bound $\mu_{k+1}^i \leq \gamma_1^i \|e_i(k\tau + \tau_0)\| \leq \gamma_1^i \gamma_0^i \mu_k^i$, $\alpha_k \neq i$, for some constant γ_1^i . Let $\gamma_1 = \max_{i=1, \dots, m} \gamma_1^i$.

Case 3: $t \in [k\tau + \tau_0, (k+1)\tau]$ and $\alpha_k = i$

Observe that if $\alpha_k = i$, the observer error dynamics for the i th subsystem are $\dot{e}_i = (A_{22}^i - L_i C_2^i) e_i = A_c^i e_i$. By designing the observer gain L_i properly, $A_c^i = A_{22}^i - L_i C_2^i$ can have n_i eigenvalues with real part less than $-a_i$ with $a_i > 0$. Under

the given τ , for some $c > 0$, $\|e^{A_c^i \tau}\| \leq c e^{-a_i \tau}$ which can be made arbitrarily small by choosing sufficiently large a_i . Consequently, $\mu_{k+1}^i \leq \gamma_c^i \|e_i(k\tau + \tau_0)\| \leq \gamma_c^i \gamma_0^i \mu_k^i$, where γ_c^i can be made arbitrarily small. Denote $\gamma_c = \max_{i=1, \dots, m} \gamma_c^i$. The actual value γ_c will be selected later to ensure convergence of the organized observer for the entire system.

In summary, combining the three cases, we have

$$\dot{e}_i = \begin{cases} A_{22}^i e_i, & t \in [k\tau, k\tau + \tau_0], \\ I_{\{\alpha_k=i\}} A_c^i e_i + I_{\{\alpha_k \neq i\}} A_{22}^i e_i, & t \in [k\tau + \tau_0, (k+1)\tau]. \end{cases}$$

It follows that the errors are bounded by $\mu_{k+1}^i \leq \gamma_k^i \mu_k^i$, with $\gamma_k^i = I_{\{\alpha_k=i\}} \gamma_c^i \gamma_0^i + I_{\{\alpha_k \neq i\}} \gamma_1^i \gamma_0^i$. Consequently, $\mu_k^i \leq (\prod_{j=1}^k \gamma_j^i) \mu_0^i$. Under *Assumption 1*, the process $\{\gamma_k^i\}$ is i.i.d. with $P(\gamma_k^i = \gamma_c^i \gamma_0^i) = p_i$, $P(\gamma_k^i = \gamma_1^i \gamma_0^i) = 1 - p_i$. The following result can be easily obtained and we omit the proof here. Subsystem observers are designed to satisfy (10).

Lemma 1: Under *Assumptions 1* and *4*, for any $\gamma_* < 1$, the pole positions in the observer design can be selected such that

$$\gamma^i = (\gamma_c^i \gamma_0^i)^{p_i} (\gamma_1^i \gamma_0^i)^{(1-p_i)} \leq \gamma_* < 1. \quad (10)$$

C. Convergence Analysis

Assumption 5: $\alpha(t)$ is independent of $e_i(0)$.

Define the continuous-time error $\mu^i(t) = \|e_i(t)\|$, which is a scalar stochastic process. Also, define $e(t) = [e_1(t), \dots, e_m(t)]^T$. The estimation error on x is $\epsilon(t) = x(t) - \hat{x}(t)$. Therefore, we can obtain the convergence results.

Theorem 2: [11] Under *Assumption 5* and the observer design in *Lemma 1*, we have (i) μ_k^i converges strongly and exponentially to 0 as $k \rightarrow \infty$; (ii) $\mu^i(t)$ converges strongly and exponentially to 0 as $t \rightarrow \infty$; (iii) $\|\epsilon(t)\|$ converges strongly and exponentially to 0 as $t \rightarrow \infty$.

VI. CASE STUDIES

A. IEEE 5-Bus system

In this subsection, we use the IEEE 5-Bus system, shown in Fig. 2, to illustrate model derivations, the design process, performance evaluation, and related issues. The power system structure and data are from the open-source information in [13]. Bus 1 and Bus 2 are dynamic dispatchable buses and Buses 3-5 are non-dynamic non-dispatchable buses.

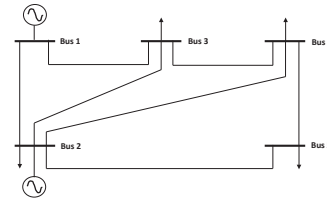


Fig. 2. IEEE 5-Bus System

In the original system, Bus 1 is a slack bus with unlimited and instantaneous power and its voltage (both magnitude and angle) is a reference point. This will significantly simplify the SHS model. In consideration of renewal generation situations under potential islanding operations (all bus angles can change dynamically during operation and no bus has unlimited power), we consider the more general scenarios and designate both Buses 1 and 2 as PV buses with bus voltage magnitudes controlled to their rated values. In light of rapid

advancement in Var compensation technology such as flexible AC transmission systems (FACTS), we assume that all buses have their voltage magnitudes maintained near the rated values during normal operations, but their values may jump during contingency.

1) Stochastic Hybrid System Models:

(i) Dynamic Systems

The most common dynamic generator types are synchronous generators [14]. Denote $\omega_1 = \dot{\delta}_1$, $z_1^d = [\delta_1; \omega_1]$, $\omega_2 = \dot{\delta}_2$, $z_2^d = [\delta_2; \omega_2]$. The dynamic systems are $M_1\dot{\omega}_1 + g_1(\omega_1) = P_1^{in} - P_1^L + P_1^{21} + P_1^{31}$, $M_2\dot{\omega}_2 + g_2(\omega_2) = P_2^{in} - P_2^L + P_2^{12} + P_2^{32} + P_2^{42} + P_2^{52}$, where the real power flow from Bus i to Bus j is $P_{ij}^j = \frac{V_j^2}{X_{ij}} \cos(\theta_{ij}) - \frac{V_i V_j}{X_{ij}} \cos(\theta_{ij} + \delta_{ij})$, and $\delta_{ij} = \delta_i - \delta_j$. The damping term $g_i(\omega_i)$ has the linear part $b_i\omega_i$ with $b_i > 0$, $i = 1, 2$. The three non-dynamic non-dispatchable buses have real-power equations $P_3^L = P_3^{13} + P_3^{23} + P_3^{43}$, $P_4^L = P_4^{24} + P_4^{34} + P_4^{54}$, $P_5^L = P_5^{25} + P_5^{45}$. Denote $z^d = [z_1^d; z_2^d]$, $z^{nd} = [\delta_3; \delta_4; \delta_5]$. The dynamic systems can be expressed as a nonlinear state equation $\dot{z}^d = F^0(z^d, z^{nd}) + B_1 v + D_1 \ell^d = F(z^d, \ell^{nd}) + B_1 v + D_1 \ell^d$, where $v = [P_1^{in}; P_2^{in}]$, $\ell^d = [P_1^L; P_2^L]$, $\ell^{nd} = [P_3^L; P_4^L; P_5^L]$, and

$$B_1 = \begin{bmatrix} 0 & 0 \\ 1/M_1 & 0 \\ 0 & 0 \\ 0 & 1/M_2 \end{bmatrix}, \quad D_1 = \begin{bmatrix} 0 & 0 \\ -1/M_1 & 0 \\ 0 & 0 \\ 0 & -1/M_2 \end{bmatrix}.$$

Denote the perturbations from the nominal values as $x = z^d - \bar{z}^d$, $u = v - \bar{v}$, $\zeta = \ell^d - \bar{\ell}^d$, $\zeta^n = \ell^{nd} - \bar{\ell}^{nd}$. By (5), the dynamic systems can be linearized near the nominal operating points as $\dot{x} = Ax + B_1 u + D_1 \zeta + D_2 \zeta^n$, where the matrices are the related Jacobian matrices $A = \left. \frac{\partial F(z^d, \ell^{nd})}{\partial z^d} \right|_{z^d = \bar{z}^d, \ell^{nd} = \bar{\ell}^{nd}}$, $D_2 = \left. \frac{\partial F(z^d, \ell^{nd})}{\partial \ell^{nd}} \right|_{z^d = \bar{z}^d, \ell^{nd} = \bar{\ell}^{nd}}$.

The nominal operating condition defined in [13], [15] is used here with the nominal bus voltages, generation powers and load powers listed in Table I with real power P (MW) and reactive power Q (MVar). The base MVA is $S_B = 100$ MVA and the base voltage is $V_B = 230$ kV. The bus line parameters, shown in Table II, are extracted from [13].

TABLE I
IEEE 5-BUS SYSTEM BUS DATA

Bus	V (p.u. \angle rad)	P	Q	P_L	Q_L
1	1.06 \angle 0	129	-7.42	0	0
2	1.0474 \angle -2.8063	40	30	20	10
3	1.0242 \angle -4.997	0	0	45	15
4	1.0236 \angle -5.3291	0	0	40	5
5	1.0179 \angle -6.1503	0	0	60	10

TABLE II
IEEE 5-BUS SYSTEM LINE PARAMETERS

Line	Resistance (p.u.)	Reactance (p.u.)	Z (p.u. $X \angle \theta$ rad)
1-2	0.02	0.06	0.06 \angle 1.25
1-3	0.08	0.24	0.25 \angle 1.25
2-3	0.06	0.25	0.26 \angle 1.33
2-4	0.06	0.18	0.19 \angle 1.25
2-5	0.04	0.12	0.13 \angle 1.25
3-4	0.01	0.03	0.03 \angle 1.25
4-5	0.08	0.24	0.25 \angle 1.25

Under the per unit system, the normalized generator parameters are $M_1 = 1.9$ and $b_1 = 0.2$ with equivalent time constant

$T_1 = M_1/b_1 = 9.5$ second for Generator 1, and $M_2 = 0.9$, $b_2 = 0.16$ with equivalent time constant $T_2 = M_2/b_2 = 5.625$ second for Generator 2. Under the aforementioned operating conditions, we obtain

$$A = \begin{bmatrix} 0 & 1 & 0 & 0 \\ 7.7926 & -0.1053 & -7.7926 & 0 \\ 0 & 0 & 0 & 1 \\ -20.3866 & 0 & 20.3866 & -0.1778 \end{bmatrix}.$$

(ii) Sensor Systems

This paper aims to present a framework in which a small number of sensors can potentially detect a large set of contingencies. For example, if a power system has 50 buses of which 10 buses are dynamic and others are non-dynamic. If each dynamic bus has a second-order state space model, then the virtual power grid model will be of order 20. It is noted that for cost reduction and maintenance simplification, it is highly desirable to reduce sensor complexity. Then a related question is: Will it be possible to use only one PMU to achieve one-line fault detection ($N - 1$ scenario) on all lines? Our algorithms indicate that this is possible, as long as the transfer functions from the control inputs to the sensor are distinct and the input is properly designed. In this simulation study, we will use the sensor that measures δ_1 (a PMU), i.e., $C = [1, 0, 0, 0]$. We will demonstrate that although this is a voltage phasor sensor, it is sufficient for detecting a line fault.

2) *Evaluation Scenarios and Input Design:* In consideration of the N-1 reliability requirements in power systems, we focus on a fault on one transmission line with different scenarios for evaluation. Line (2,3) which is the longest transmission line in the system, is selected. The line faults are characterized by jumps in the impedance values X_{23} . Four cases are considered: (1) Normal Operation: $\alpha = 1$: $X_{23} = 0.26$, with probability $p_1 = 0.9$; (2) Line Fault 1 (Reduced Impedance): $\alpha = 2$: $X_{23} = 0.1$, with probability $p_2 = 0.06$; (3) Line Fault 2 (single line to ground fault): $\alpha = 3$: $X_{23} = 0.06$, with probability $p_3 = 0.03$; (4) Line Fault 3 (Disconnection): $\alpha = 4$: $X_{23} = 10000$, with probability $p_4 = 0.01$.

The corresponding A matrices are :

$$A(1) = \begin{bmatrix} 0 & 1 & 0 & 0 \\ 7.7926 & -0.1053 & -7.7926 & 0 \\ 0 & 0 & 0 & 1 \\ -20.3866 & 0 & 20.3866 & -0.1778 \end{bmatrix},$$

$$A(2) = \begin{bmatrix} 0 & 1 & 0 & 0 \\ 7.7967 & -0.1053 & -7.7967 & 0 \\ 0 & 0 & 0 & 1 \\ -20.5843 & 0 & 20.5843 & -0.1778 \end{bmatrix},$$

$$A(3) = \begin{bmatrix} 0 & 1 & 0 & 0 \\ 7.7978 & -0.1053 & -7.7978 & 0 \\ 0 & 0 & 0 & 1 \\ -20.6409 & 0 & 20.6409 & -0.1778 \end{bmatrix},$$

$$A(4) = \begin{bmatrix} 0 & 1 & 0 & 0 \\ 7.7571 & -0.1053 & -7.7571 & 0 \\ 0 & 0 & 0 & 1 \\ -18.6540 & 0 & 18.6540 & -0.1778 \end{bmatrix},$$

respectively. It is easy to verify that under $C = [1, 0, 0, 0]$, the corresponding observability matrices $W(1)$, $W(2)$, $W(3)$, $W(4)$ are full rank. As a result, the stochastic hybrid system

has observable subsystems. For this reason, state decomposition is not needed, and we will directly estimate x under each detected subsystem.

We first calculate the eigenvalues of $A(i)$ and obtain their eigenvalues, which are $\{-5.388, 5.2302, 0, -0.1253\}$, $\{-5.407, 5.2491, 0, -0.1252\}$, $\{-5.412, 5.2545, 0, -0.1251\}$, $\{-5.2181, 5.0616, 0, -0.1266\}$. Since they share the common eigenvalue 0, an input is needed to detect different systems. Select $u = a \sin t$ with $a > 0$, which satisfies the conditions of Theorem 1 (namely, $U(s) = \frac{a}{s^2+1}$, Assumption 3 is satisfied). By using a small a , this probing signal will have a negligible impact on the system's normal operation. For this case study, $a = 0.1$ is used, although smaller values of a can still work.

3) Results and Discussions:

(i) Detection of Subsystems

As an example, taking $\tau = 2.5$ and $\tau_0 = 0.05$, we show the detection of α_0 for $t \in [0, \tau_0)$. Suppose the initial state is $[2, -1, 1, 2]$, and the true $\alpha_0 = 1$. Now we estimate α_0 by Algorithm 1. Under the probing input $u(t) = 0.1 \sin(t)$, Fig. 3 shows the curve of $u(t)$ and $y(t)$. According to Algorithm 1, we calculate the output prediction errors of the four subsystems, then we obtain $\varepsilon_1 = 2.7464 \times 10^{-14}$, $\varepsilon_2 = 1.6518 \times 10^{-9}$, $\varepsilon_3 = 2.1253 \times 10^{-9}$, $\varepsilon_4 = 1.4480 \times 10^{-8}$. Therefore, $\hat{\alpha}_0 = 1$, which detects the subsystem accurately.

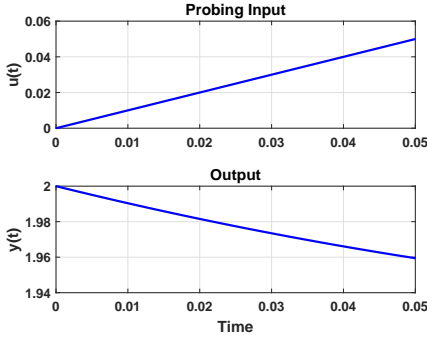


Fig. 3. The probing input $u(t)$ and the output $y(t)$ in $[0, \tau_0)$.

(ii) Observer Design and Convergence

The pole placement design is used for designing observer feedback gains. For example, if we choose the desired closed-loop poles as $\lambda = [-4.8, -3.6, -4, -4.4]$, then the Matlab function $L_i = \text{place}(A^\top(i), C^\top, \lambda)$, $i = 1, 2, 3, 4$, yields the suitable feedback gains and the closed-loop error dynamics with $A_c^i = A(i) - L_i C$, $i = 1, 2, 3, 4$.

Take $\tau = 2.5$ and $\tau_0 = 0.05$. The initial estimation error is selected to be $e(0) = [2, -1, 1, 2]^\top$ with the error norm $\sqrt{10}$. Fig. 4 shows that α_k can be accurately detected and the estimation error is convergent.

(iii) Robustness against Measurement Errors

We now consider measurement noise and show the impact of output measurement errors on contingency detection accuracy. For the one-sensor case (i.e., $C = [1, 0, 0, 0]$), suppose that the standard deviation is $\sigma = 0.005$, and the measured output value is $\hat{y} = y + \sigma d$, where d is the noise with uniform distribution in $[-0.5, 0.5]$. Take $\tau = 2.5$, $\tau_0 = 0.05$, $\lambda =$

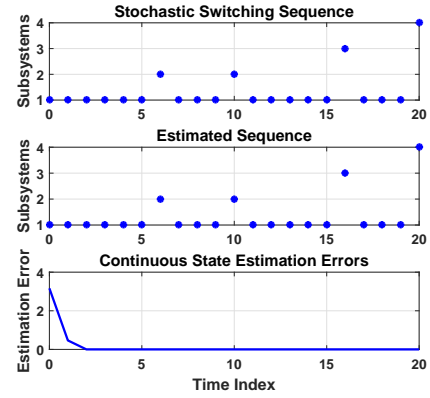


Fig. 4. The detection of α_k and the estimation error trajectory.

$[-4.8, -3.6, -4, -4.4]$. Fig. 5 shows that α_k can still be accurately detected. However, the steady-state error is big.

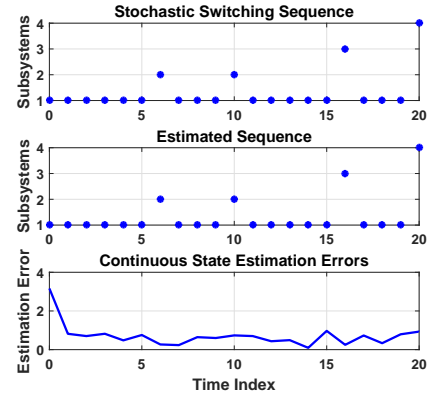


Fig. 5. The detection of α_k and the estimation error trajectory.

If we use two sensors δ_1 and δ_2 , i.e., $C = \begin{bmatrix} 1 & 0 & 0 & 0 \\ 0 & 1 & 0 & 0 \end{bmatrix}$. Suppose $\sigma = 0.005I_2$, then under the same τ and τ_0 , and the same pole positions, the steady-state error becomes smaller, see Fig. 6.

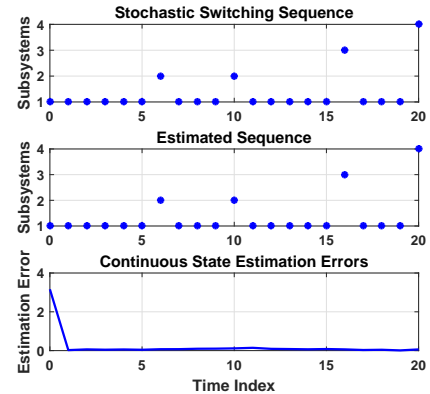


Fig. 6. The detection of α_k and the estimation error trajectory.

B. IEEE 33-Bus system

To elucidate our algorithms in a more comprehensive context, we utilize the IEEE 33-bus system [16], [17] as an illustrative example in our research.

1) Modeling and Linearization of the IEEE 33-Bus System:

The original 33-bus system [16] contains one slack bus tied to the large grid and the rest buses are PQ-type load buses. For evaluation of renewable systems, more local generators have been added. Following the enhanced 33-bus evaluation system proposed in [18], in this simulation study, Bus 1 remains as a slack bus and two generators are added, at Bus 18 and Bus 33, shown in Fig. 7. The generator buses are dynamic buses whose local state space models for real power management are represented by their swing equations. All other buses remain as PQ-type load buses as in the original configuration and non-dynamic. The slack bus voltage is set as the reference bus with constant voltage $1\angle 0$ (pu), whose P and Q injections are unlimited and instantaneous in balancing powers in each step. Consequently, the slack bus is non-dynamic. All bus and load parameters are from the power flow data in [16] and obtained from the 33-bus case file in MATPOWER [17], [19], [20]. The base power of the IEEE 33-bus system is 100 (MW) and the base voltage is $V_B = 230$ (kV).

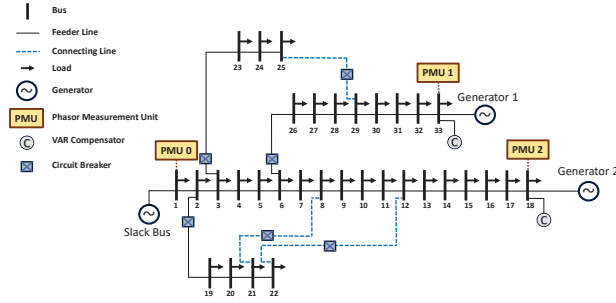


Fig. 7. The enhanced IEEE 33-bus distribution test system.

The nonlinear dynamic models for Bus 18 and Bus 33 are summarized below. Denote $\omega_{18} = \dot{\delta}_{18}, \omega_{33} = \dot{\delta}_{33}$. The dynamic systems are

$$\begin{aligned} M_{18}\dot{\omega}_{18} + g_{18}(\omega_{18}) &= P_{in}^{18} - P_{out}^{18}, \\ M_{33}\dot{\omega}_{33} + g_{33}(\omega_{33}) &= P_{in}^{33} - P_{out}^{33}, \end{aligned}$$

where P_{out}^i is the total transmitted power from Bus i to its neighboring buses. Denote the line admittance $Y_{ij} = |Y_{ij}|\angle\gamma_{ij}$ and shunt admittance $Y_i = |Y_i|\angle\gamma_i$.

Since Bus 18 (and Bus 33) has only one neighboring Bus 17 (and Bus 32), we have

$$P_{out}^{18} = V_{18}^2|Y_{18}| \cos(\gamma_{18}) + V_{18}V_{17}|Y_{18,17}| \cos(\delta_{18} - \delta_{17} - \gamma_{18,17}),$$

and similarly for Bus 33. The damping term is assumed to be linear with $b_{18} = 0.22, b_{33} = 0.12$. The normalized inertias are $M_{18} = 1.8$ and $M_{33} = 0.9$.

Dynamic interactions of generators with the power grid are different from the traditional power flow analysis and introduce a new iteration scheme. During the transient time, $P_{in}^{18} \neq P_L^{18} + P_{out}^{18}$ which drives changes in δ_{18} . The new δ_{18} then enters power flow analysis to result in new power flow status, including the new P_{out}^{18} ; similarly for Bus 33. As a result, during transient calculation of the power flow status, we designate the 66 dependent variables in power flow calculation via MATPOWER as $Z = [P_{out}^d, Q_{out}^d, P_s, Q_s, V^{nd}, \delta^{nd}]$, where the superscript d refers to the dynamic buses 18 and 33, nd refers to the load buses 2 – 17 and 19 – 32, and the subscript s refers to the slack bus 1.

Under the generation powers $P_{in}^{18} = 1.29$ pu and $P_{in}^{33} = 0.89$ pu, the equilibrium point (the stationary operating condition) is calculated as $\bar{\delta}_{18} = -0.01$ (degree), $\bar{\omega}_{18} = 0$, $\bar{\delta}_{33} = 0.12$ (degree), $\bar{\omega}_{33} = 0$. The slack bus provides real power 3.94 pu. The corresponding values of Z at the equilibrium point are denoted by \bar{Z} .

Denote $x = (\delta_{18}, \omega_{18}, \delta_{33}, \omega_{33})$, $u = [P_{in}^{18}, P_{in}^{33}]$, the state equation is $\dot{x} = f_0(x, G(\delta_{18}, \delta_{33}), u) = f(x, u)$. Then the Jacobian matrix at the equilibrium point $x = \bar{x}, Z = \bar{Z}$ is

$$A = \left. \frac{\partial f_0(x, Z, u)}{\partial x^T} \right|_{x=\bar{x}, Z=\bar{Z}} + \left. \frac{\partial f_0(x, Z, u)}{\partial Z} \right|_{x=\bar{x}, Z=\bar{Z}} \frac{\partial Z}{\partial x^T} \Big|_{x=\bar{x}, Z=\bar{Z}}.$$

Based on the actual expressions of $f(x, u)$, the Jacobian matrix is given by

$$A = \begin{bmatrix} 0 & 1 & 0 & 0 \\ -\frac{1}{M_{18}} \frac{\partial P_{out}^{18}}{\partial \delta_{18}} & -\frac{b_{18}}{M_{18}} & -\frac{1}{M_{18}} \frac{\partial P_{out}^{18}}{\partial \delta_{33}} & 0 \\ 0 & 0 & 0 & 1 \\ -\frac{1}{M_{33}} \frac{\partial P_{out}^{33}}{\partial \delta_{18}} & 0 & -\frac{1}{M_{33}} \frac{\partial P_{out}^{33}}{\partial \delta_{33}} & -\frac{b_{33}}{M_{33}} \end{bmatrix}.$$

Utilizing the initial 33-bus power flow data sourced from [16], [17]² and employing MATPOWER for power flow analysis along with the computation of partial derivatives, we obtain

$$A = \begin{bmatrix} 0 & 1 & 0 & 0 \\ -1.1280 & -0.1222 & -0.0120 & 0 \\ 0 & 0 & 0 & 1 \\ -0.0344 & 0 & -4.4785 & -0.1333 \end{bmatrix}.$$

2) *Evaluation Scenarios and Input Design:* Let the line impedance of line (i, j) be denoted by $X_{i,j}$. Three cases are considered: (1) Normal Operation: $\alpha = 1$: $X_{1,2} = 0.05753$ and $X_{26,27} = 0.17732$, with probability $p_1 = 0.9$; (2) Line Fault 1 (Increased Impedance of line (1,2)): $\alpha = 2$: $X_{1,2} = 0.5753$, with probability $p_2 = 0.06$; (3) Line Fault 2 (Increased Impedance of line (26,27)): $\alpha = 3$: $X_{26,27} = 1.7732$, with probability $p_3 = 0.04$. The corresponding $A(i)$ matrices are :

$$\begin{aligned} A(1) &= \begin{bmatrix} 0 & 1 & 0 & 0 \\ -1.1280 & -0.1222 & -0.0120 & 0 \\ 0 & 0 & 0 & 1 \\ -0.0344 & 0 & -4.4785 & -0.1333 \end{bmatrix}, \\ A(2) &= \begin{bmatrix} 0 & 1 & 0 & 0 \\ -1.1281 & -0.1222 & -0.0127 & 0 \\ 0 & 0 & 0 & 1 \\ -0.0386 & 0 & -4.4877 & -0.1333 \end{bmatrix}, \\ A(3) &= \begin{bmatrix} 0 & 1 & 0 & 0 \\ -1.1277 & -0.1222 & -0.0115 & 0 \\ 0 & 0 & 0 & 1 \\ -0.0299 & 0 & -4.5179 & -0.1333 \end{bmatrix}. \end{aligned}$$

We first calculate the eigenvalues of $A(i)$ and obtain their eigenvalues, which are $\{-0.0611 + 1.0602i, -0.0611 - 1.0602i, -0.0667 + 2.1152i, -0.0667 - 2.1152i\}$, $\{-0.0611 + 1.0603i, -0.0611 - 1.0603i, -0.0667 + 2.1174i, -0.0667 - 2.1174i\}$, $\{-0.0611 + 1.0601i, -0.0611 - 1.0601i, -0.0667 + 2.1245i, -0.0667 - 2.1245i\}$. Select $u = 0.1 \sin t$ as the probing input, which satisfies the conditions of Theorem 1.

²For the original data for the buses, links, generators, and loads of the 33-bus system, please refer to the case33 file in MATPOWER, see [19], [20].

3) Results and Discussions:

(i) Detection of Subsystems

Take $\tau = 4.5$ and $\tau_0 = 0.9$. We show the detection of α_0 for $t \in [0, \tau_0)$ as an example. Suppose the initial state is $[-1, 2, 1, 2]$, and the true $\alpha_0 = 1$. Now we estimate α_0 by Algorithm 1. Under the probing input $u(t) = 0.1 \sin(t)$, Fig. 8 shows the curve of $u(t)$ and $y(t)$. According to Algorithm 1, we calculate the output prediction errors of the four subsystems, then we obtain $\varepsilon_1 = 7.5964 \times 10^{-13}$, $\varepsilon_2 = 8.1380 \times 10^{-5}$, $\varepsilon_3 = 2.4539 \times 10^{-4}$. Therefore, $\hat{\alpha}_0 = 1$, which detects the subsystem accurately.

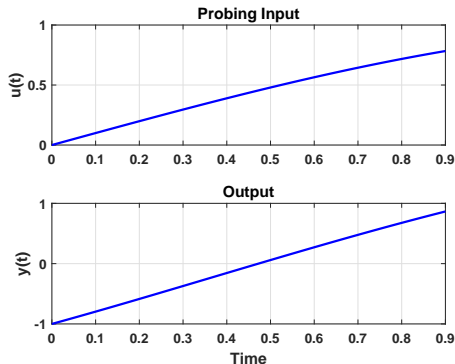


Fig. 8. The probing input $u(t)$ and the output $y(t)$ in $[0, \tau_0)$.

(ii) Observer Design and Convergence

We suppose that the sensor is on δ_{18} , i.e., $C = [1, 0, 0, 0]$. The pole placement design is used for designing observer feedback gains. If we choose the desired closed-loop poles as $\lambda = [-4, -3.2, -4.8, -4.4]$, then the Matlab function $L_i = \text{place}(A^\top(i), C^\top, \lambda)$, yields the suitable feedback gains and the closed-loop error dynamics with $A_c^i = A(i) - L_i C$, $i = 1, 2, 3$.

Take $\tau = 4.5$ and $\tau_0 = 0.9$. The initial estimation error is selected to be $e(0) = [-1, 2, 1, 2]^\top$ with the error norm $\sqrt{10}$. Fig. 9 shows that α_k can be accurately detected and the estimation error is convergent. It should be pointed out that one sensor can identify different line faults.

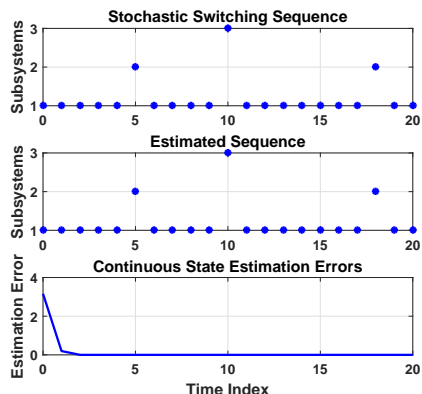


Fig. 9. The detection of α_k and the estimation error trajectory.

(iii) Packet Delivery

Suppose that δ_1 and δ_2 are independently measured. Denote $C(1) = \begin{bmatrix} 1 & 0 & 0 & 0 \\ 0 & 0 & 1 & 0 \end{bmatrix}$ for normal operation, $C(2) = [1, 0, 0, 0]$

for failure of Sensor 2 (δ_1 measurement only), $C(3) = [0, 0, 1, 0]$ for failure of Sensor 1 (δ_2 measurement only), and $C(4) = [0, 0, 0, 0]$ for failure on both sensors. Suppose that the packet delivery ratio for Sensor 1 is $\rho_1 = 0.95$ and for Sensor 2 is $\rho_2 = 0.97$. This data acquisition scheme can be modeled by an i.i.d. stochastic process $\alpha_k \in \mathcal{S} = \{1, \dots, 4\}$ with $p_1 = \rho_1 \rho_2 = 0.9215$, $p_2 = \rho_1(1 - \rho_2) = 0.0285$, $p_3 = (1 - \rho_1)\rho_2 = 0.0485$, $p_4 = (1 - \rho_1)(1 - \rho_2) = 0.0015$.

The pole placement design is used for designing observer feedback gains for $\alpha_k = 1, 2, 3$. Since $C(4) = 0$, the observer can only run open-loop. For example, if we choose the desired closed-loop poles as $\lambda = [-1, -0.8, -1.2, -1.5]$, then the Matlab function $L_i = \text{place}(A', C'(i), \lambda)$, yields the suitable feedback gains and the closed-loop error dynamics with $A_c^i = A - L_i C(i)$, $i = 1, 2, 3$.

Take $\tau = 5$ and $\tau_0 = 1$. The initial estimation error is selected to be $e(0) = [-1, 2, 1, 2]^\top$ with the error norm $\sqrt{10}$. Fig. 10 shows that α_k can be accurately detected and the estimation error is convergent.

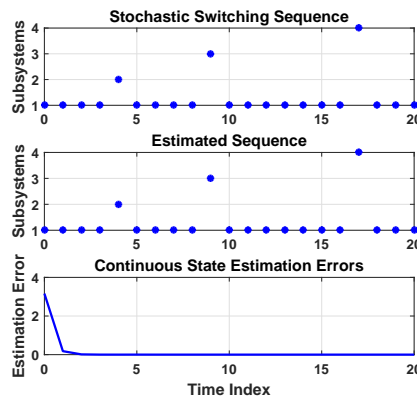


Fig. 10. The detection of α_k and the estimation error trajectory.

VII. CONCLUDING REMARKS

This paper introduced a new approach to contingency detection in MPS. The approach employs a stochastic hybrid system model in the state space form that captures both jumps from contingencies and internal dynamics of continuous states. Since system dynamics contain rich information on changes of system structures and parameters, the same output measurements for normal power system operation such as PMUs, frequencies, voltages, etc. can be used to detect contingencies of different types, causes, and locations. Model derivations, input design, detection algorithms, state estimation, and their stability and convergence properties were established. Practical bus systems were used to demonstrate the results.

REFERENCES

- [1] D. P. Kothari and I. J. Nagrath, *Modern Power System Analysis*, McGraw Hill Higher Education, 2008.
- [2] M. Singh, B. K. Panigrahi, and R. P. Maheshwari, "Transmission line fault detection and classification," in *2011 International Conference on Emerging Trends in Electrical and Computer Technology*, Nagercoil, India, 2011, pp. 15-22.
- [3] G. S. Nandakumar, V. Sudha, and D. Aswini, "Fault detection in overhead power transmission," *International Journal of Pure and Applied Mathematics*, vol. 118, no. 8, pp. 377-381, 2018.

- [4] Y. K. Fu, "Electrical line fault detection and line cut-off equipment and control," *Journal of Control Science and Engineering*, vol. 2022, pp. 1-6, 2022.
- [5] S. Yuan, L. Y. Wang, G. Yin, and M. Nazari, "Stochastic hybrid system modeling and state estimation of modern power systems under contingency," under review, 2023.
- [6] P. Gopakumar, M. J. B. Reddy, and D. K. Mohanta, "Transmission line fault detection and localisation methodology using PMU measurements," *IET Generation, Transmission & Distribution*, vol. 9, no. 11, pp. 1033–1042, 2015.
- [7] K. Chen, J. Hu, and J. He, "Detection and classification of transmission line faults based on unsupervised feature learning and convolutional sparse autoencoder," *IEEE Transactions on Smart Grid*, vol. 9, no. 3, pp. 1748–1758, May 2018.
- [8] S. Affijulla and P. Tripathy, "A robust fault detection and discrimination technique for transmission lines," *IEEE Transactions on Smart Grid*, vol. 9, no. 6, pp. 6348–6358, Nov. 2018.
- [9] M. Gholami, A. Abbaspour, M. Moeini-Aghtaie, M. Fotuhi-Firuzabad, and M. Lehtonen, "Detecting the location of short-circuit faults in active distribution network using PMU-based state estimation," *IEEE Transactions on Smart Grid*, vol. 11, no. 2, pp. 1396–1406, March 2020.
- [10] L. Y. Wang, G. Yin, F. Lin, M. P. Polis, and W. Chen, "Stochastic observability and convergent analog state estimation of randomly switched linear systems with unobservable subsystems," *IEEE Transactions on Automatic Control*, vol. 68, no. 2, pp. 898-911, Feb. 2023.
- [11] L. Y. Wang, G. Yin, F. Lin, M. P. Polis, and W. Chen, "Joint estimation of continuous and discrete states in randomly switched linear systems with unobservable subsystems," *IEEE Transactions on Automatic Control*, 2022.
- [12] J. D. Glover and M. S. Sarma, *Power System Analysis and Design*, 3rd Edition, Brooks Cole, Thomson Learning, Inc., 2001.
- [13] R. Tan, IEEE 5-Bus System Model (<https://www.mathworks.com/matlabcentral/fileexchange/66555-ieee-5-bus-system-model>), MATLAB Central File Exchange, 2023.
- [14] P. S. Kundur, *Power System Stability and Control*, 1st Edition, McGraw Hill, 1994.
- [15] A. A. Bhandakkar and L. Mathew, "Real-time-simulation of IEEE-5-Bus network on OPAL-RT-OP4510 simulator," in *3rd International Conference on Communication Systems (ICCS-2017)*, Rajasthan, India, 2017, pp. 14–16.
- [16] M. E. Baran and F. F. Wu, "Network reconfiguration in distribution systems for loss reduction and load balancing," *IEEE Trans. Power Del.*, vol. 4, no. 2, pp. 1401–1407, Apr. 1989.
- [17] J. Y. Wong, "IEEE 33 Bus System," 2020, MATLAB Central File Exchange. Accessed: Sep. 15, 2020. [Online]. Available: <https://www.mathworks.com/matlabcentral/fileexchange/73127-ieee-33-bus-system>.
- [18] S. H. Dolatabadi, M. Ghorbanian, P. Siano, and N. D. Hatziaargyriou, "An Enhanced IEEE 33 Bus Benchmark Test System for Distribution System Studies," *IEEE Transactions on Power Systems*, vol. 36, no. 3, pp. 2565–2572, May 2021.
- [19] R. D. Zimmerman, C. E. Murillo-Sanchez, and R. J. Thomas, "MATPOWER: Steady-state operations, planning, and analysis tools for power systems research and education," *IEEE Transactions on Power Systems*, vol. 26, no. 1, pp. 12–19, Feb. 2011.
- [20] R. D. Zimmerman and C. E. Murillo-Sanchez, "Matpower [software]," 2018. [Online]. Available: <https://matpower.org>